Journal of Template

Vol. 00, No. 0, 0000

Laminar-Turbulent Transition of an Inlet Boundary Layer in a Circular Pipe Induced by Periodic Injection (Shape of Isolated Turbulent Patches and Their Growth)*

Masashi ICHIMIYA**, Hayato MATSUDAIRA***, Hayato FUJIMURA*** and Hideki OHNO***

**Institute of Technology and Science, The University of Tokushima

2-1 Minami-Josanjima-cho, Tokushima-shi, Tokushima, 770-8506 Japan

E-mail: ichimiya@tokushima-u.ac.jp

***Graduate School, The University of Tokushima

Abstract

The laminar-turbulent transition of a boundary layer induced by a jet injection in the inlet region of a circular pipe was experimentally investigated. The jet was periodically injected radially from a small hole in the inlet region into the pipe flow. Axial velocity was measured by a hot-wire anemometer. The turbulence induced by the jet within the boundary layer developed into turbulent patches which then grew in the axial, circumferential and radial directions downstream. The shape of the patches shown by the intermittency factor in the diametrical plane was similar to the turbulent spot in the flat plate boundary layer at first, then became similar to the turbulent slug in the pipe flow developed downstream. The turbulent patches protruded from the boundary layer after they grew and reached the circumferential opposite side, although they stayed within the boundary layer as long as the shape was turbulent spot-like in the diametrical plane. The propagation velocity at the leading edge became faster than the cross-sectional velocity, though it turned slower at the trailing edge. Therefore, the growth rate of its axial length varied downstream. The growth rate of the patches' circumferential length was smaller than that in the turbulent spot under zero pressure gradient and was almost the same as the spot under favorable pressure gradient.

Key words: Pipe Flow, Transition, Boundary Layer, Turbulence, Inlet Region, Isolated Turbulent Patch, Propagation Velocity, Turbulent Spot

1. Introduction

Fully developed laminar pipe flow (Hagen-Poiseuille; HP flow) has been shown to be stable in infinitesimal disturbances from theoretical and experimental studies[(1)~(4)]. As is well known, however, if the Reynolds number exceeds a threshold level (1800－2300), isolated turbulent patches (turbulent puffs or slugs) originate intermittently. They occupy the whole cross section and their axial length grows downstream, then the flow always shows turbulence finally. The contradiction between the above fact and the linear stability theory is attributed to an ignorance of two factors in the theory; finite amplitude disturbance and upstream inlet (entrance) region. The latter has been shown to be unstable in finite Reynolds number. Therefore, the role that the inlet region plays in the laminar-turbulent

*Received XX Xxx, 200X (No. XX-XXXX)
[DOI: 00.0000/ABCDE.2006.000000]

transition is significant, and is expected to be elucidated. Recently, Mullin stated that since the inlet region is more sensitive to the disturbances than the HP flow, it is important to control the inlet disturbance[5]. He also stated that since in practical pipes flow comes in with background disturbance or is easy to separate and become unstable due to acute edges in an entrance, the inlet flow is important from an application standpoint. At present, however, investigations about the inlet flow are less than those of HP flow.

The present authors have conducted experiments that introduced a disturbance to the inlet laminar flow and studied the steady turbulent region formed downstream of three-dimensional single roughness element on the wall, and revealed its properties[6]. Next, isolated turbulent patches were generated by a jet injected perpendicularly to the pipe flow from a hole in the wall[7]. The threshold flow rate of the jet to create the turbulence was examined as a function of the Reynolds number and jet duration, leading to different results from the HP flow. The velocity signals within the turbulent patches were also shown and the effects of the jet flow rate and injection frequency on the axial length and internal velocity fluctuation in the turbulent patches were examined.

However, after their generation, the shape of the isolated turbulent patches, their spreading nature and relative position within the inlet boundary layer have not been clarified. Unlike the HP flows, uniform flow without vorticity, the core region presents in the outer boundary layer within the inlet region as well as the flat plate boundary layer. Therefore, the characteristic of isolated turbulence patches that occur in the boundary layer are expected to be similar to the turbulent spots of flat plate boundary layer rather than the turbulent puffs or slugs in a developed circular pipe. The elucidation of the details may contribute to elucidate the role of inlet flow plays in the turbulent transition in circular pipe flows.

So far, the main facts elucidated by experiments about turbulent puffs or slugs in HP flow are as follows: Whereas the puffs occur at low Reynolds number with high disturbances, the slugs occur at high Reynolds number with low disturbances[8]. The leading (downstream) edge is unclear, but the trailing (upstream) edge is clear in the puffs[8]~[13]; on the other hand, both edges are clear in the slugs[8][10][12]. Propagation velocity of the leading edge is faster than the cross-sectional average velocity, whereas that of the trailing edge is slower than the cross-sectional average velocity. The difference extends the length of the slugs downstream[8][12]. Among several theoretical and numerical studies of the puffs and slugs, a new model has been proposed recently[14].

Many studies of turbulent spots in the flat plate boundary layer have also been conducted. The main elucidated points are as follows: Their shape on a plane parallel to the wall protrudes outside (downstream direction) at the leading edge, but is recessed inside at the trailing edge. The leading edge lifted from the wall and overhung the central cross-section[15][16]. Although the leading edge is clear, on the other hand, within the trailing edge the flow gradually returns to the laminar flow and a calmed region exists[15][16]. The propagation velocity at the leading edge is faster than that at the trailing edge, making streamwise length extend downstream. The propagation velocity remains constant downstream at both edges under zero pressure gradient[17]~[22], but increases under a favorable pressure gradient[23][24]. When the origin and the transverse outer edge are connected, they become a straight line. The half of the spreading angle of 9°－11° under zero pressure gradient[15][17][21], is smaller under the favorable pressure gradient[25][26] and is larger under an adverse pressure gradient[26]~[28].

In order to clarify the still non-defined characteristics of the isolated turbulent patch in the inlet region in a circular pipe, in this study the isolated turbulent patch generated periodically in the inlet region was measured also in the inlet region as in the previous report. Then the shape of the turbulent patch, and its relative position within the boundary layer and the growth in three directions were examined. In addition, these characteristics

were compared with the turbulent puffs or slugs in HP flow or turbulent spots in a flat plate boundary layer.

2. Experimental Apparatus and Methods

The experimental apparatus is the same one used in the previous paper[7]. A plexiglas pipe with a diameter, $D = 2a$, of 60 mm and a total length of approximately 6.2 m (= $104D$) was used in the experiments. A fan downstream of the pipe sucked air into the pipe. Six pipes 1 m in length each are connected smoothly. The axial velocity was axisymmetric. For the convenience of the reader, the coordinate system and flow field are reproduced in Fig. 1. As a point disturbance, a single jet flow was injected perpendicularly to the main flow through a 2-mm diameter hole 107 mm downstream of the coordinate origin, as shown in Fig. 1.

In the present study, in order to inject the jet periodically, air emitted from an air pump is led to a solenoid valve. In the control signal of the solenoid valve, periodically generated rectangular voltage from a photo-interrupter is led to the valve. The injection duration is 0.1 seconds, but the non-injection duration, t_{j2}, is 0.3 or 0.7 seconds; therefore, the combination time of jet flow injection and non-injection, T_j, is 0.4 or 0.8 seconds. For measurements not too far downstream from the jet hole $(x-x_j)/D \leqq 19.2$, the non-injection duration is 0.3s. On the other hand, for downstream $26.1 \leqq (x-x_j)/D$, since the turbulent patch elongates, the non-injection duration is extended to 0.7s in order not to merge adjacent patches.

The Reynolds number based on the pipe diameter and the velocity averaged over the cross-section, U_a, is kept at 10000 ($U_a \simeq 2.5$ m/s). This value is lower than the critical Reynolds number in the inlet region based on the linear stability theory by Tatsumi[29], Huang and Chen[30] and Gupta and Garg[31] (19400, 39800 and 23400, respectively, based on a pipe diameter and cross-sectional average velocity). It is shown in the previous report that the threshold flow rate of the jet to generate the isolated turbulent patch depends on the injection duration and Reynolds number[7]. In this report, the jet flow rate was set to 6.3×10^{-6} m^3/s (jet speed $v_j = 2.0$ m/s) which sufficiently exceeds the threshold flow rate at $Re = 10000$. That is, in this experiment a finite amplitude disturbance is inserted into a stable region in line with the linear stability theory of the inlet region. At this time, the ratio of flow rate, momentum per unit time and momentum flux (momentum per unit time and unit area) between the jet and main flow are 9×10^{-4}, 8×10^{-4} and 0.7, respectively. When the jet is not injected in the pipe, the inlet region continues over the whole pipe length[7].

A single hot-wire probe with a tungsten sensing element 5 μm in diameter and 1 mm in length was used in an axial velocity measurements. The output voltage from the hot wire had been digitized at a 10 kHz sampling frequency and a 52-second sampling period. An ensemble averaging based on the output voltage from the photointerrupter was performed. The sampling period corresponds to 130 and 65 times of the ensemble average in the region of $(x-x_j)/D \leqq 19.2$ ($T_j = 0.4$ s) and $26.1 \leqq (x-x_j)/D$ ($T_j = 0.8$ s), respectively. When the ensemble average number exceeds about 50, the difference of various quantities with

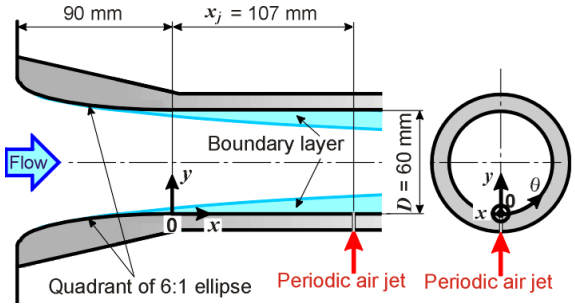

Fig. 1 Coordinate system and air jet.

the average number disappeared. In the Ref. (12) 60 times of the ensemble average was conducted.

Results are shown here in the axial stations within $(x-x_j)/D$ = 2.5, 3.5, 9.4, 14.9, 19.2, 26.1, 31.6, 35.8 and 42.7. When the jet is injected, these stations are still within the inlet region as will be shown in Fig. 6. A pipe of 150 mm in length including the jet injection hole is adapted to rotate around its center axis. That makes it possible to select the desired circumferential measurement position, θ, relative to the hole. The finest interval in the circumferential position was 5°. Only the station of $(x-x_j)/D$ = 9.4 in both ranges of -180° $\leqq \theta \leqq$ 0° and 0° $\leqq \theta \leqq$ 180°, were measured. Since the symmetry with respect to the center position θ = 0° was good as described later, in the other stations only a region of 0° $\leqq \theta \leqq$ 180° was measured. Forty-three radial positions were measured in the region of 0.2 mm $\leqq y \leqq$ 30 mm.

To distinguish the flow as laminar or turbulent, in the present experiment a one-order time derivative of axial fluctuating velocity is compared with a constant threshold value which has been judged as valid from many comparisons between the discrimination results and instantaneous velocity signals. The previous report showed all distributions of the velocity and the wall static pressure without the jet injection[7].

3. Results and Discussion

3.1 Shape of Turbulent Patch

In this section, the intermittency contour maps were used to examine the downstream variation of the shape of the turbulent patch at nine stations in the inlet region. First of all, the instantaneous and local flow was discriminated as turbulent or non-turbulent, then the intermittent function $I(\tilde{t}, x, y, \theta)$ was set as unity or zero in the turbulent or non-turbulent flow, respectively, where $\tilde{t}$ is an instantaneous time. The ensemble average of this function, $\langle I \rangle$, is shown in Fig. 2. Although the time-averaged intermittent function, $\gamma(x, y, \theta)$, is usually called the intermittency factor, in this paper the ensemble-averaged one, $\langle I \rangle(t, x, y, \theta)$, is called the intermittency factor for convenience. Since this ensemble averaging is performed about the lapsed time from the jet injection time, t ($0 \leqq t < T_j$), the period of the ensemble average is the same as that of the jet injection, T_j. As a criterion for the outline of the flat-plate turbulent spots, based on the ensemble-averaged mean velocity, $U + \langle u \rangle$, the position whose value changes as $\pm 0.02U_\infty$ (U_∞ is the mainstream speed) from the laminar flow velocity outside has often been used[17][20][32]. Otherwise, based on a deviation from the ensemble-averaged velocity, i.e., irregularly fluctuating intensity, u', the position where this becomes $0.02U_\infty$ also has been used[33][34]. For the trailing edge, Glezer et al. showed that the use of a half-intermittency is more suitable[35]. Though the present study adopted the half-intermittency, "$\langle I \rangle$ = 0.5", the shape of the turbulent patch based on the present method and on "u'/U_e = 0.02", was comparable near the pipe center axis. On the other hand, near the pipe wall the region based on the present method became smaller, and on the border of half-intermittency the fluctuation increased to u'/U_e = 0.1.

In Fig. 2, intermittency contour maps are shown on diametrical planes which pass through the jet hole (θ = 0°, y = 0), the pipe center axis and the wall of θ = 180°. Therefore, the development of the turbulent patch in the streamwise and radial directions can be observed. In each figure the lower half ($0 \leqq y/a \leqq 1$) and an upper half ($1 \leqq y/a \leqq 2$) are θ = 0° and 180° sides, respectively. The numerical value in the ordinate is a height measured from the surface of the jet-hole side (θ = 0°) wall normalized by the pipe radius. In the abscissa, instead of the axial coordinate, x, a lapsed time normalized by velocity averaged over the cross section and a pipe diameter, $T = U_a(t + nT_j)/D$ (n is an integer, $0 \leqq t < T_j$), is used. At a location not to far downstream of the turbulence, the patch is within a

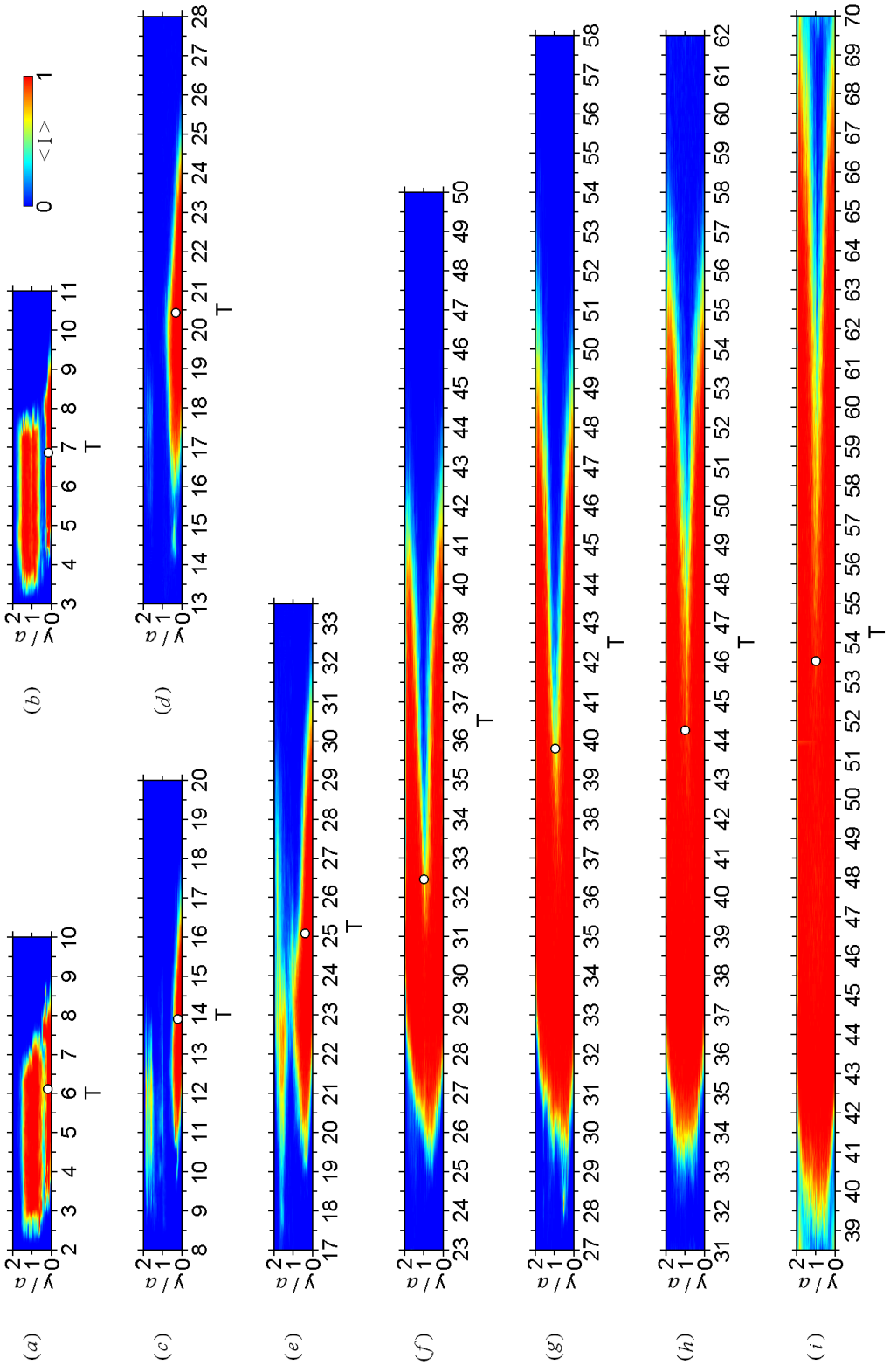

Fig. 2 Intemittency contour maps on diametrical plane. (*a*) $(x-x_j)/D = 2.5$; (*b*) $(x-x_j)/D = 3.5$; (*c*) $(x-x_j)/D = 9.4$; (*d*) $(x-x_j)/D = 14.9$; (*e*) $(x-x_j)/D = 19.2$; (*f*) $(x-x_j)/D = 26.1$; (*g*) $(x-x_j)/D = 31.6$; (*h*) $(x-x_j)/D = 35.8$; (*i*) $(x-x_j)/D = 42.7$.

small *T* area. On the other hand, the patch arrives downstream later, so it is within a large *T* area. The downstream interface i.e., leading edge of the patch passes the hot-wire probe fixed in space first, and finally the upstream interface i.e., trailing edge passes. Therefore, the increase in the non-dimensional lapsed time, *T*, from the jet injection time corresponds

to the passing of the observation time of the hot-wire probe. This means going back upstream spatially from the leading toward the trailing edges within the patch. That is, in each contour map of Fig. 2(*a*)-(*i*), the left (small *T*) side is the leading edge side, while the right (large *T*) side is the trailing edge side. In flat-plate turbulent spots, non-dimensional coordinate $\xi = (x - x_j) / (U_\infty t)$ is used as similarity coordinate in many cases[18]. Under the zero pressure gradient where the velocity at the leading and trailing edges are kept constant, the ξ range of the spots becomes constant irrespective of x and is a convenient display. In the present turbulent patch, however, since both velocities change downstream as mentioned later, the display by ξ is not so appropriate. Thus, the non-dimensional lapsed time, *T*, was used in this study. The increase in a turbulent patch's duration is reflected in the increase in *T* range. Although the range of *T* drawn is almost within the surrounding laminar flow range before and after the patch, it was limited to the range which is equivalent to one period T_j at the maximum. Since the leading edge velocity increases and the trailing edge velocity decreases as it goes downstream as mentioned later, the patch does not necessarily pass through the position x in each figure with a constant length shown in Fig. 2. The details will be given in §3.3.

Moreover, as a guide of the center of the turbulent patch, the center of gravity whose intermittency factor is regarded as mass on the diametrical plane was shown in Fig. 2 by the open circles. The intermittency factor was interpolated and calculated in every $0.01 U_a T_j / D$ in the *T* direction and in every 1/300 in the *y*/*a* direction, then the center of gravity was obtained from the following equations using $\langle I \rangle_i$ at each point:

$$T_c = \frac{\sum_i \langle I \rangle_i T_i}{\sum_i \langle I \rangle_i} \quad , \quad y_c = \frac{\sum_i \langle I \rangle_i y_i}{\sum_i \langle I \rangle_i}. \tag{1}$$

Where the subscript *i* shows the data point number for the interpolation. Though at $(x - x_j) / D$ = 2.5 and 3.5, two turbulent patches are shown in the pipe wall (θ = 0°) side and upper part (pipe center side) as mentioned later, since the one in the pipe wall side grows downstream, the center of gravity is shown only in this patch.

Downstream variation of the turbulent patch is seen below. First, at $(x - x_j) / D$ = 2.5 (Fig. 2(*a*)), the patch can be seen in the range of 2.5 < *T* < 8.5. Although the patch is beginning to separate into the pipe wall (θ = 0°) part and upper part, the non-turbulent flow, $\langle I \rangle$ = 0, does not divide both patches completely.

At $(x - x_j) / D$ = 3.5 (Fig. 2(*b*)), the range of *T* where the patch exists changed to 3.5 < *T* < 9.5, and this shows that the patch propagated downstream. Although the upper patch shifts further upward, the one in the pipe wall (θ = 0°) side remains near the wall as ever, and is separated completely from the upper one.

Farther downstream, at $(x - x_j) / D$ = 9.4 (Fig. 2(*c*)), the range of the upper patch becomes small. On the other hand, the one in the wall (θ = 0°) side still exists near the wall, and the streamwise and radial range increases. Therefore, the turbulent patch is judged to be the jet itself which is injected from the jet hole perpendicularly to the pipe flow. Since the jet rises and enters the pipe core without velocity gradient, it is expected to disappear. For the core range, the boundary layer thickness was shown in Figs. 5 and 6 later. The *T* range based on the jet injection duration, t_{j1} = 0.1 s, that is, the normalized time for the streamwise advance of the turbulent patch with the velocity U_a during 0.1 seconds, is approximately 4.3. This time almost corresponds to the region of the upper patch in Figs. 2 (*a*) and (*b*). Of course, since the range seems to reduce during the advance of 2.5*D* or 3.5*D* in the streamwise direction, this correspondence is a mere guide. Moreover, when the patch is assumed to rise in the radial direction with the jet injection velocity, v_j, during the streamwise advance time of 2.5*D* or 3.5*D*, the raised height was estimated to be 1.9*D* or 2.8*D*, respectively. Since the upper turbulent patch in Fig. 2(*a*) and (*b*) has not reached even

such height, it turns out that the injected jet is considerably bent in the streamwise direction by the pipe mainstream. The locus of the bent jet was estimated according to Ref. (36) using the velocity ratio between the jet and mainstream $a = v_j / U_a \simeq 0.8$ in this experiment. In fact, its radial position had merely the same order of magnitude as the upper turbulent patch in Fig. 2(*a*) and (*b*). The reason for the exact disagreement might be that the jet immediately after the injection exists in the boundary layer near the wall where the velocity ratio is larger than 0.8.

On the other hand, the turbulent patch in the wall ($\theta = 0°$) side is considered to have been induced by the jet. Since the wall-side patch exists in the boundary layer as the flat-plate turbulent spot, it grows. The spatial relationship of the patch and the boundary layer thickness is examined in Fig. 6. The jet immediately after the injection pulsated at 60 Hz equal to the air pump driving frequency[7]. The 60-Hz periodicity remained in the turbulent patch at $(x-x_j)/D = 2.5$ and $y/a = 0.03$[7]. It corresponds to the patch in the pipe wall ($\theta = 0°$) side in Fig. 2(*a*). In addition, of course, the 60-Hz periodicity was observed in the velocity in the upper patch. Farther downstream, at $(x-x_j)/D = 9.4$, although the upper patch damped considerably as mentioned above, the 60-Hz periodicity still remained. On the other hand, in the patch in the wall ($\theta = 0°$) side the periodicity was extinguished[7]. That is, while the upper patch which is the jet itself keeps the 60-Hz periodicity, it advances at least 9.4*D* in the streamwise direction. On the other hand, although the turbulent patch in the pipe wall ($\theta = 0°$) side keeps the 60-Hz periodicity at 2.5*D* downstream, irregular velocity fluctuation increases immediately since it exists within the boundary layer, and the periodicity will be extinguished before it reaches 9.4*D*.

At $(x-x_j)/D = 14.9$ (Fig. 2(*d*)), the upper patch has disappeared completely, and one in the wall ($\theta = 0°$) side has grown sufficiently long in the streamwise direction. The radial range is the widest near the center of gravity.

At $(x-x_j)/D = 19.2$ (Fig. 2(*e*)) the top of the patch reaches the pipe center axis, and the patch begins to appear near the pipe wall ($\theta = 180°$). This means that the patch developed in the circumferential direction reached 180°. Later this development will be explained with the contour maps in the cross-section in Fig. 3. The leading edge of the patch is projected toward downstream, and overhung the wall. On the other hand, the trailing edge is not overhung. This form is similar to the turbulent spots in the flat plate boundary layer[15]. The position where the radial range is the widest is closer to the leading edge rather than the center-of-gravity position.

At $(x-x_j)/D = 26.1$ (Fig. 2(*f*)), the grown-up patch exists in not only the $\theta = 0°$ side but also the 180° side, and both merge where the radial range is the widest and covers the whole radial range $0 \leqq y/a \leqq 2$ in the region of $29 \leqq T \leqq 31.5$. Then, from here, the

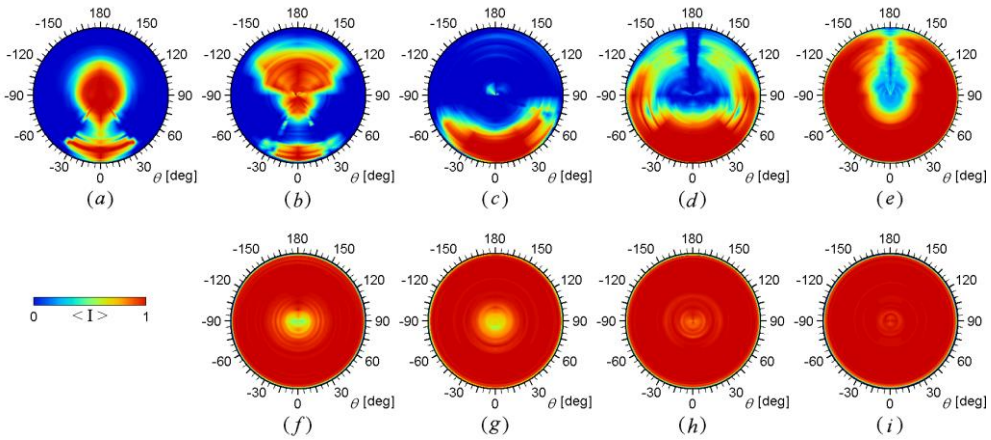

Fig. 3 Intermittency contour maps on cross sections at center of intermittency. (*a*) $(x-x_j)/D = 2.5$; (*b*) $(x-x_j)/D = 3.5$; (*c*) $(x-x_j)/D = 9.4$; (*d*) $(x-x_j)/D = 14.9$; (*e*) $(x-x_j)/D = 19.2$; (*f*) $(x-x_j)/D = 26.1$; (*g*) $(x-x_j)/D = 31.6$; (*h*) $(x-x_j)/D = 35.8$; (*i*) $(x-x_j)/D = 42.7$.

center of gravity was calculated within the range including the $\theta = 180°$ side. Thus, the measurements sufficiently covered downstream after the turbulence patch occupied the whole section. The axial length of the patch extending up to $\theta = 180°$ is still shorter than that on the $\theta = 0°$ side. Hence, the patch at the leading edge is not completely symmetrical with respect to the pipe center axis.

At $(x-x_j)/D$ = 31.6, 35.8 and 42.7 (Fig. 2(*g*), (*h*) and (*i*)), the patch grows further in the axial direction. Moreover, the leading and trailing edge are also symmetrical with respect to the pipe center axis. The leading edge of the present turbulent patch projects downstream; on the other hand, the trailing edge is depressed, tapering inside like turbulent slugs[8]. The shape can be explained in that the two patches approach from the upper and lower sides in the figure and merge in at the radially thickest *T* position, though the trailing edge has not merged yet.

From here, the development of the turbulent patch in the circumferential direction is examined. Figure 3 shows the intermittency contour maps in the cross section perpendicular to the pipe axis at the center of gravity time. The jet injection hole $\theta = 0°$ is the bottom position in each figure. The jet was injected from that position upward. Although the half circumferential range $0° \leqq \theta \leqq 180°$ (right half of each figure) was measured except for $(x-x_j)/D$ = 9.4 (Fig. 3(*c*)), the maps are drawn for the whole circumferential range by drawing the left half symmetrically.

At $(x-x_j)/D$ = 2.5 (Fig. 3(*a*)) the turbulent patch induced by the jet injected $\theta = 0°$ can be observed in the range of $-40° \leqq \theta \leqq 40°$. The jet itself is observed near the pipe center axis. At $(x-x_j)/D$ = 3.5 (Fig. 3(*b*)), the circumferential range of the turbulent patch near the wall becomes smaller. The upper jet rises for a little height, as in Fig. 2(*b*). Farther downstream $(x-x_j)/D$ = 9.4 (Fig. 3(*c*)), the patch in the wall side further spreads in the circumferential direction; on the other hand, the upper turbulent patch has disappeared in the center-of-gravity time shown in Fig. 3(*c*). Only in this station the whole circumferential range was measured. The symmetry of the intermittency factor with respect to $\theta = 0°$ is well. The radial range of the turbulent patch is the widest at $\theta = 0°$.

Farther downstream, the spreading of the turbulent patch in the circumferential direction continues, then connects with the opposite side of itself at $\theta = 180°$ and spans the entire periphery in the cross section. Next, it gradually thickens also radially, finally seeming cover the whole cross-sectional area. In fact, with reference to Fig. 2, the cross section is totally covered with the patch at the center-of-gravity time.

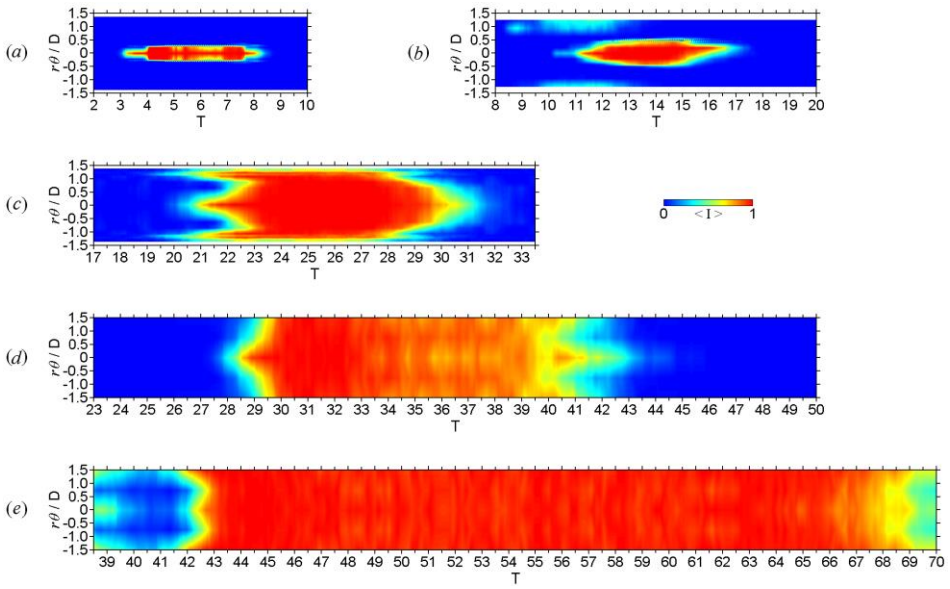

Fig. 4 Intermittency contour maps on concentric cylindrical plane. (*a*) $(x-x_j)/D$ = 2.5; (*b*) $(x-x_j)/D$ = 9.4; (*c*) $(x-x_j)/D$ = 19.2; (*d*) $(x-x_j)/D$ = 26.1; (*e*) $(x-x_j)/D$ = 42.7.

Figure 4 shows the turbulent patch at a fixed height expanded in plan views in five typical stations. At $(x-x_j)/D$ = 2.5, 9.4 and 19.2 (Fig. 4(*a*), (*b*) and (*c*)), the intermittency contour maps are cut at y/a = 0.13, 0.20 and 0.17, respectively, where in Fig. 3 at the center of gravity the range of $\langle I \rangle$ = 0.5 is the widest periphery. On the other hand, at $(x-x_j)/D$ = 26.1 and 42.7 (Fig. 4(*d*) and (*e*)), where the turbulent patch has reached up to $\theta = 180°$, the contour maps are cut at y/a = 0.04 and 0.05, respectively, where the *T*-direction average of the rms value of the irregular fluctuation, *u*', within the patch is maximum. The ordinate is the circumferential distance $r\theta = (a-y)\theta$ normalized by the pipe diameter. Thus, the circumferential position where the jet hole exists, i.e., the symmetry axis $\theta = 0°$ corresponds to $r\theta = 0$. Also in Fig. 4, as in Fig. 3, the $r\theta \leqq 0$ side are drawn to be symmetrical with the pipe center axis.

In the region of $(x-x_j)/D \leqq 19.2$, where the turbulent patch is in the form of a flat-plate turbulent spot in the diametrical plane, Fig. 2, the leading and trailing edges are projected to the outside together in the axis of symmetry $\theta = 0°$ in Fig. 4. That is, although the leading edge form is the turbulent spot type, the trailing edge form is not a turbulent spot type depressed inside. Even in the region $26.1 \leqq (x-x_j)/D$, where the form became a turbulent slug type in the diametrical plane, the form that projected outside in the axis of symmetry does not change.

3.2 Relationship of Mean Flow Quantities within Isolated Turbulent Patch and Inlet Boundary Layer

In this section the relationship between the mean flow quantities within the isolated turbulent patch and inlet boundary layer is discussed. Radial distributions of the ensemble-averaged velocity in representative *T* at three axial stations are shown in Fig. 5. The normalized time, *T*, where the distributions are drawn in the respective figure, are: laminar flow outside of the turbulent patch, near the leading edge of the patch, the inside of the patch, and near the trailing edge of the patch. Vertical lines are drawn in the position of the selected *T*. For example, in Fig. 5(*a*) the distributions are drawn at *T* = 3, 6, 8 and 9. With reference to Fig. 2, the position of the turbulent patch can be identified. Also, in Fig. 5, in *T* of laminar flow, theoretical distributions in inlet laminar boundary layer of Tatsumi[37] are also drawn in red lines. Moreover some radial extent is magnified. Tatsumi gave the velocity against the height from the pipe wall normalized by the displacement thickness. In

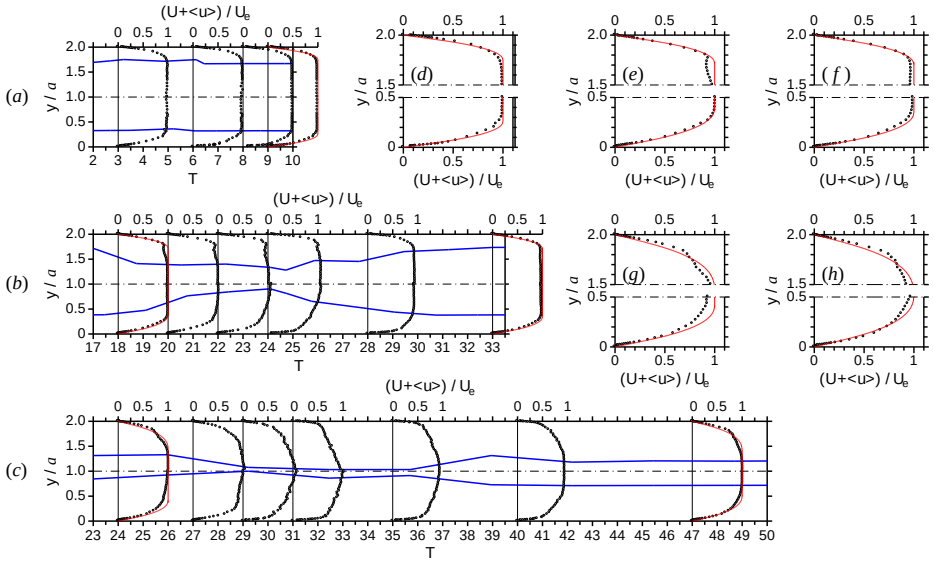

Fig. 5 Ensemble-averaged velocity profiles and boundary layer thickness on diametrical plane. (*a*) $(x-x_j)/D$ = 2.5; (*b*) $(x-x_j)/D$ = 19.2; (*c*) $(x-x_j)/D$ = 26.1; (*d*) $(x-x_j)/D$ = 2.5, *T* = 9; (*e*) $(x-x_j)/D$ = 19.2, *T* = 18; (*f*) $(x-x_j)/D$ = 19.2, *T* = 33; (*g*) $(x-x_j)/D$ = 26.1, *T* = 24; (*h*) $(x-x_j)/D$ = 26.1, *T* = 47. Red line, Tatsumi profile; blue line, boundary layer thickness.

this study, using the experimental values of displacement thickness in each $(x-x_j)/D$ and T, the theoretical distributions were drawn. Therefore, distributions vary depending on $(x-x_j)/D$ and T. In the previous report[7], the time-averaged velocity distributions without the jet injection were in good agreement with the Tatsumi distribution over the whole pipe length, so the flow was completely laminar.

Although the laminar flow upstream shown in Fig. 5 is close to the Tatsumi profile, the difference with the Tatsumi profile is remarkable in the enlargement near the wall (Fig. 5 (*g*) and (*h*)) as it goes downstream since the laminar flow gradually begins a natural transition. The natural transition process has been explained in the previous report[7]. In the core outside the boundary layer, however, the profile is in agreement with the Tatsumi profile. Compared with profiles of the laminar flow in the same axial stations, the profile within the turbulent patch is faster near the wall and slower away from the wall. Moreover, within the patch the profile just behind the leading edge is not smooth. This means that the deviation from the ensemble-averaged value in each patch is quite large. Distributions of the deviation, i.e., the irregular fluctuation will be considered in the future. Moreover, the boundary layer thickness, $<\delta>$, defined as the height at which the ensemble-averaged velocity becomes 0.995 times the maximum in the radial distribution, is shown in blue lines on both ($\theta = 0°$ and 180°) sides, the thickness has been calculated in every $1.6T$ at $(x-x_j)/D$ = 2.5 and 19.2 and in every $3.2T$ at $(x-x_j)/D$ = 26.1. Note that the boundary-layer thickness at T where the velocity profile is drawn is the position of the blue line not at the intersection of the symbols but at the intersection of the normal line. At $(x-x_j)/D$ = 2.5 (Fig. 5(*a*)), although inside the turbulent patch near the wall there is a velocity gradient, the velocity is constant near the center axis, thus showing that the existence of the gradient governs a subsequent turbulent patch development as mentioned above. At $(x-x_j)/D$ = 19.2 and 26.1 (Fig. 5(*b*) and (*c*)), where only the patch near the wall persists, the velocity gradient exists within the patch.

Next, the spatial relationship of the turbulent patch and the boundary layer is examined. Figure 6 shows the boundary layer thickness, $<\delta>$, of $\theta = 0°$ and 180° drawn in the white lines on five intermittency contour maps chosen from Fig. 2. At the most downstream station, $(x-x_j)/D$ = 42.7 (Fig. 6(*e*)), since the boundary layer does not reach the pipe center axis in any time T, the station is therefore within the inlet region.

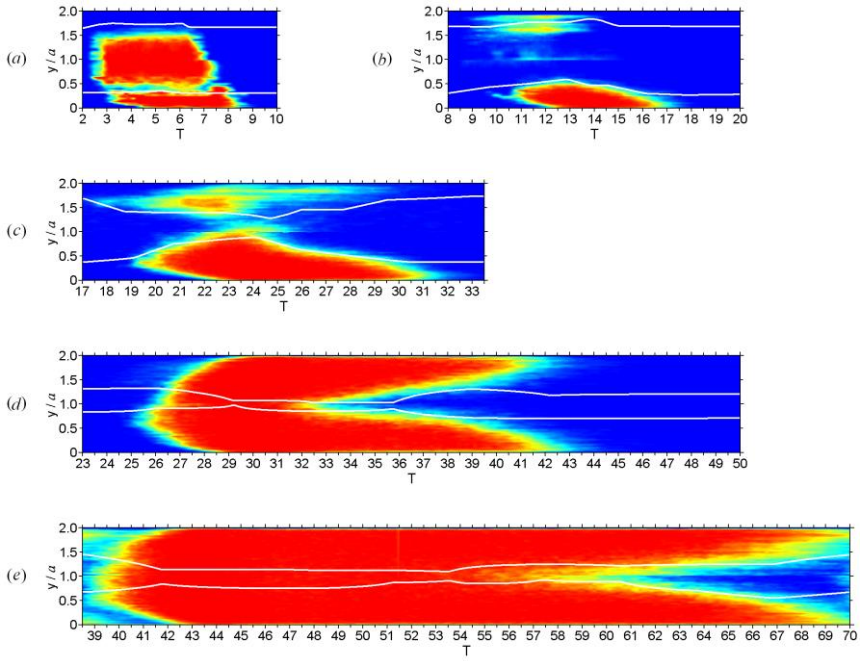

Fig. 6 Ensemble-averaged boundary layer thickness on diametrical plane. (*a*) $(x-x_j)/D$ = 2.5; (*b*) $(x-x_j)/D$ = 9.4; (*c*) $(x-x_j)/D$ = 19.2; (*d*) $(x-x_j)/D$ = 26.1; (*e*) $(x-x_j)/D$ = 42.7.

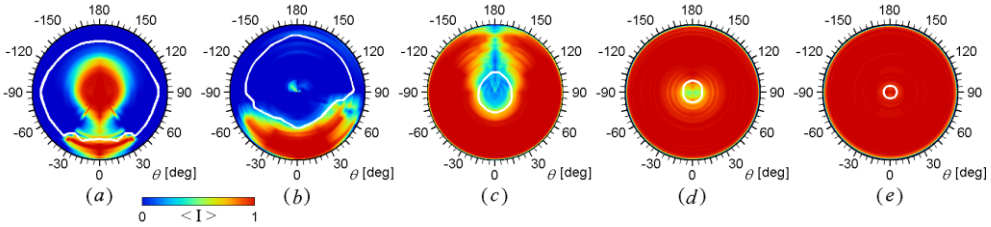

Fig. 7 Ensemble-averaged boundary layer thickness on cross sections at center of intermittency. (*a*) $(x-x_j)/D = 2.5$; (*b*) $(x-x_j)/D = 9.4$; (*c*) $(x-x_j)/D = 19.2$; (*d*) $(x-x_j)/D = 26.1$; (*e*) $(x-x_j)/D = 42.7$.

The turbulent patch remains almost within the boundary layer at $(x-x_j)/D \leqq 19.2$ (Fig. 6(*a*), (*b*) and (*c*)), though it runs through the boundary layer and reaches the center axis at $(x-x_j)/D = 26.1$ (Fig. 6(*d*)) where it spreads in the circumferential direction and is connected at $\theta = 180°$. Considering the fact that the height of the flat-plate turbulent spot is comparable to that of a turbulent boundary layer whose height at the origin is the same as a laminar boundary layer there[17], the present turbulent patch is thicker than the flat-plate turbulent spot.

Figure 7 shows the boundary layer thickness in the center-of-gravity time on five cross sections with the intermittency contour maps in Fig. 3 so that it may be easy to understand the spatial relationship with the turbulent patch. At $(x-x_j)/D = 2.5$ and 9.4 (Fig. 7(*a*) and (*b*)), where the turbulent patch has not spread enough in the circumferential direction, the boundary layer is thick in the circumferential position where the patch exists, but thin outside the patch. The circumferential growth of the turbulent patch is quicker than that in the boundary-layer-thickness direction, i.e., the radial direction. In the radial direction the existence of the velocity gradient $\partial U / \partial y$ within the boundary layer causes the circumferential component of a vorticity, Ω_θ. The vorticity in the shape of a closed ring along with the periphery within the boundary layer makes for easy transmission of the velocity and vorticity fluctuations in the circumferential direction. On the other hand, the lack of velocity gradient in the core region outside of the boundary layer makes it difficult for the fluctuations to be transmitted in the radial direction.

3.3 Growth of Turbulent Patch

In this section the growth of the isolated turbulent patch in the axial, circumferential and radial directions is discussed quantitatively. Figure 8 shows the axial variation of the above-mentioned most downstream leading edge time, center of intermittency time, and most upstream trailing edge time. For $(x-x_j)/D \leqq 3.5$, only the turbulent patch near the wall is considered. The slope of the dashed line in Fig. 8 is unity, which means that $(x-x_j)/t \sim U_a$, i.e., going on axial distance $x-x_j$ with the cross-sectional average velocity, U_a, between the time t. Although the slope of the leading edge is close to unity at first and mostly propagates with U_a, the slope increases gradually and the leading edge propagates faster than U_a. On the other hand, the slope of the trailing edge decreases gradually and the trailing edge propagates slower than U_a. This velocity difference of the leading and trailing edges makes the axial length of the turbulent patch, i.e., the distance between T_l and T_t in given $(x-x_j)/D$ gradually longer. The axial length will be shown in Fig. 10 later. The virtual origins of the most downstream leading and most upstream trailing edges almost correspond to T = zero and $U_a\, t_{j1}/D = 4.3$ ($t_{j1} = 0.1$ s), respectively.

Next the propagation velocities in the leading and trailing edges are shown to be made dimensionless by the cross-sectional average velocity. For example, the leading edge velocity, U_l, is obtained from the distance between two axial stations divided by the difference in the arrival time of the leading edge, $t_l = T_l D/U_a$, at the two stations. The leading edge velocity is normalized by the cross-sectional average velocity, and then is shown at the middle point of the two stations. However, since the Reynolds number is fixed,

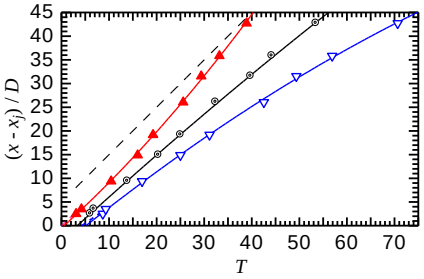

Fig. 8 Downstream variation of most downstream leading edge (▲), center of intermittency (◎) and most upstream trailing edge (▽). broken line, $(x-x_j)/D \sim T$.

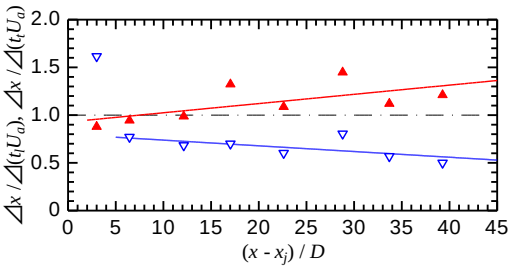

Fig. 9 Propagation velocity. ▲, leading edge; ▽, trailing edge; red line, $\Delta x / \Delta(t_l U_a) \sim 0.0097(x-x_j)/D$; blue line, $\Delta x / \Delta(t_t U_a) \sim -0.0060(x-x_j)/D$.

the kinematic viscosity and also the average velocity vary with the stations. Therefore, the distance is divided by the difference of $t_l U_a$ between two stations, while $\Delta x/\Delta(t_l U_a)$ is shown in Fig. 9 as the normalized leading edge propagation velocity in practice. The propagation velocity in the trailing edge is also obtained similarly. Two solid lines in Fig. 9 are straight lines fitted by the least squares method from eight leading edge stations and seven excluding the uppermost of trailing edge stations, respectively.

Although the trailing edge is faster than the leading edge at first, the leading edge exceeds the trailing edge immediately. Then, the leading edge gradually becomes faster than the cross-sectional average velocity and the trailing edge becomes slower than the average velocity. The difference in both edges increases downstream, and it does not converge on a constant value in the measured range. This fact differs from the propagation velocity of the flat-plate turbulent spots under a zero pressure gradient[17)~(22)]. Moreover, the condition is also different from the flat-plate turbulent spots under the favorable pressure gradient in which the propagation velocities on both edges increase downstream[23)(24)]. The propagation velocity of the leading and trailing edges are larger and smaller than the cross-sectional averaged velocity, respectively, in the turbulent puffs and slugs in HP flow; the condition is in agreement with present turbulent patch. In the turbulent puffs or slugs the difference of both propagation velocities increases downstream[12)]. In the most downstream station in this experiment, the normalized leading and trailing edge velocity are equivalent to those in HP flow with the Reynolds number of approximately 5000. That is, the difference of propagation velocity at both edges in the present turbulent patch in the inlet region is smaller than that in HP flow with the same Reynolds number.

Figure 10 shows the axial variation of the turbulence patch's axial length. This length is obtained from the difference in arrival time of the trailing edge and that of the leading edge, (t_t-t_l) times the propagation velocity of the trailing edge, U_t, or that of the leading edge, U_l, obtained from Fig. 9. These two lengths correspond to the turbulent patch's axial length when its leading edge (blue symbols in Fig. 10) or trailing edge (red symbols in Fig. 10) arrives at station x, respectively. Since the propagation velocities, U_t and U_l, change in the axial direction as shown in Fig. 9, at fixed x both propagation velocities are also changing continuously during a period of (t_t-t_l). Therefore, the variation of both propagation velocities with T is first obtained from Figs. 8 and 9; next they are converted into the change with the time t, and from an integration with time from t_l to t_t the axial lengths are obtained finally. In Fig. 9, the region of $(x-x_j)/D \leqq 6$ where the propagation velocity of the trailing edge significantly differs from the blue solid line is excluded. Since the height of the leading and trailing edges are not necessarily equal, the length l_x is not on a constant height. The quantity shown in Fig. 10, however, can be a guide to the turbulent patch length.

First, we consider Fig. 10(a) shown with the linear coordinates. Although the axial length of the turbulent patch shown in the red triangles shrunk from $(x-x_j)/D = 2.5$ to 3.5, it immediately begins to extend significantly. This proves that in Fig. 9, although the

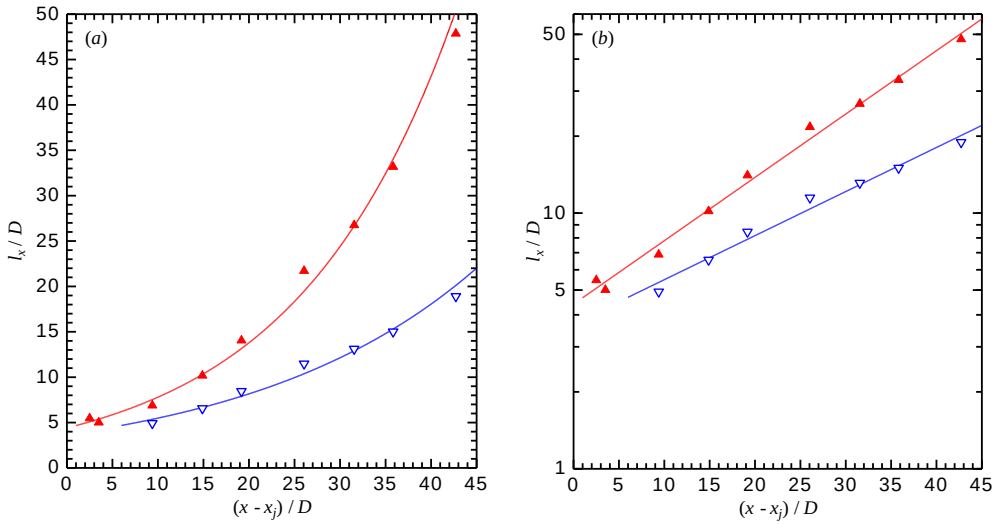

Fig. 10 Axial growth of turbulent patches. (*a*) Linear expression; (*b*) Semi-logarithmic expression; red line, $l_x / D = 4.41\exp\{0.0570(x-x_j) / D\}$; blue line, $l_x / D = 3.69\exp\{0.0397(x-x_j) / D\}$.

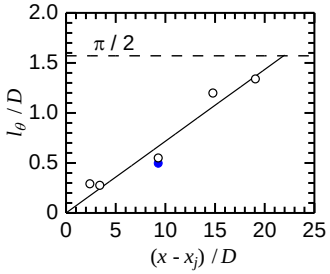

Fig. 11 Circumferential growth of turbulent patches. solid line, $l_\theta = 0.072(x-x_j)$; ●, negative θ.

propagation velocity of the leading edge is initially slower than that of the trailing edge, it exceeds it immediately. Since the reduction of the patch is limited to within a few periods and afterwards begins to grow, it is the growing stage that is mainly considered. This growth rate is increasing downstream, i.e., the patch does not show linear growth. When the leading edge arrives at the station furthest downstream of $(x-x_j)/D = 42.7$, the axial length is approximately 19D from Fig. 10(*a*). This means that the trailing edge exists approximately 19D upstream, i.e., at $(x-x_j)/D \simeq 24$. In fact, when the trailing edge exists in $(x-x_j)/D = 24$, the axial length is also approximately 19D from Fig. 10(*a*) and they correspond well. At the furthest downstream station $(x-x_j)/D = 42.7$, the difference in length when the leading and trailing edges arrive there is approximately 29D. This means its length more than doubles until the patch passes that location. This fact suggests that the growth of the turbulent patch in this experiment is a result of the convective instability. Though data were still in a curve in a log-log plot (not shown) usually tried in this kind of expression, the semi-log plot in Fig. 10(*b*) clearly shows that a straight-line approximation can be carried out. That is, the length of the turbulent patch increases exponentially. Two straight lines in Fig. 10(*b*) are obtained by the least-squares method. Taking $\eta = (x-x_j)/D$, we obtain $d\,l_x / d\eta = k\,l_x$ (k is a constant). This shows that the convective spatial growth is a type with a spatial growth rate proportional to l_x itself.

Next, the growth in the circumferential direction is examined. From the intermittency contour maps on the cross section in the center-of-gravity time in Fig. 3, the one side circumferential length of turbulent patch, i.e., the widest circumferential region of $\langle I \rangle = 0.5$, i.e., half-intermittency is shown in Fig. 11. Therefore, the height of the circumferential length changes with $(x-x_j)/D$. At $(x-x_j)/D = 19.2$, where the turbulent patch reaches a circumferential position of $\theta = 180°$, the circumferential length is obtained from an extrapolation of the region of the half-intermittency. This length is not along the pipe wall,

so the value at $(x-x_j)/D$ = 19.2 does not exceed $(\pi/2)D$. At $(x-x_j)/D$ = 9.4, both circumferential ($0° \leqq \theta$ and $\theta \leqq 0°$) lengths are shown. As seen in Fig. 4(*a*), (*b*) and (*c*), since the circumferential range of the turbulent patch is almost constant in a wide range of T including center-of-gravity, the circumferential length is shown in the center-of-gravity time as representative.

The circumferential length increases in the downstream direction linearly. The five points (only positive θ region in $(x-x_j)/D$ = 9.4) are fitted to a least square straight line and shown in Fig. 11. From a slope of the straight line of 0.072, the half spread angle in the circumferential direction is estimated as approximately 4 degrees. This value is smaller than in the turbulent spots in a zero-pressure-gradient flat-plate boundary layer (9°－11°)[15][17][21] and is comparable to that in a favorable-pressure-gradient flat-plate boundary layer (6° or less[23] or 3°－4°[24]).

4. Conclusions

An isolated turbulent patch was generated by a periodical jet injection into an inlet region of a circle pipe. The shape, spatial relationship with a boundary layer and growth in three directions of the patch were examined in the inlet region, and the following conclusions were obtained.

(1) The jet itself, which was injected perpendicularly to the flow rises as is, enters the core and finally disappears. On the other hand, the disturbance induced within the boundary layer becomes an isolated turbulent patch, and downstream it grows in the axial, circumferential and radial directions.

(2) The shape in a diametrical plane of the turbulent patch in intermittency contour maps is similar to the turbulent spots in a flat-plate boundary layer at first. Downstream it resembles the turbulent slugs in the circular pipe in a developed region whose leading edge sharpens toward the downstream and the trailing edge depressed toward its inside. Within a plane parallel to the pipe wall, the shape is not similar to the turbulent spot. The leading and trailing edges always project outside on the axis of symmetry.

(3) The patch grows in the circumferential direction quicker than in the radial direction. While the shape in the diametrical plane is the flat-plate turbulent spot type, it remains within the boundary layer. After reaching the opposite position of the periphery, it runs through a boundary layer and reaches the pipe center.

(4) The propagation velocity of the leading and trailing edges of the patch shows different downstream change from the flat-plate turbulent spots. As it proceeds downstream, the propagation velocity at the leading or trailing edges gradually becomes faster or slower than the cross-sectional average velocity, respectively. Moreover, compared with the turbulent puffs and slugs in the Hagen-Poiseuille flow of the same Reynolds number, the difference in the propagation velocity in the leading and trailing edges is smaller.

(5) An axial length of the turbulent patch increases exponentially in the axial direction. The spatial extension rate is proportional to the axial length of the axial station itself. The circumferential length increases linearly. The spreading rate is smaller than that of the turbulent spots in a flat plate boundary layer under a zero pressure gradient and comparable under a favorable pressure gradient.

Acknowledgments

The authors appreciate the kind instruction and constant encouragement of Prof. I. Nakamura, Nagoya University. The generous assistance of Messrs. H. Nishida, M. Funaki and K. Satou of the University of Tokushima is also gratefully acknowledged.

References

(1) Kerswell, R. R., Recent Progress in Understanding the Transition to Turbulence in a Pipe, *Nonlinearity*, Vol. 18, No. 6 (2005), pp. R17-R44.
(2) Eckhardt, B., Schneider, T. M., Hof, B., and Westerweel, J., Turbulence Transition in Pipe Flow, *Annual Review of Fluid Mechanics*, Vol. 39 (2007), pp. 447-468.
(3) Eckhardt, B., Turbulence Transition in Pipe Flow: Some Open Questions, *Nonlinearity*, Vol. 21, No. 1 (2008), pp. T1-T11.
(4) Willis, A. P., Peixinho, J., Kerswell, R. R., and Mullin, T., Experimental and Theoretical Progress in Pipe Flow Transition, *Philosophical Transactions of the Royal Society*, A, Vol. 366 (2008), pp. 2671-2684.
(5) Mullin, T., Experimental Studies of Transition to Turbulence in a Pipe, *Annual Review of Fluid Mechanics*, Vol. 43 (2011), pp. 1-24.
(6) Ichimiya, M., Abe, T., Fukutomi, J., and Kondo, M., Laminar-Turbulent Transition of a Boundary Layer Induced by a Single Roughness Element in an Inlet Region of a Circular Pipe Flow (Developing Process of a Stationary Turbulent Region), *Transactions of the Japan Society of Mechanical Engineers, Series B*, Vol. 73, No. 725 (2007), pp. 154-161 (in Japanese).
(7) Ichimiya, M., Fujimura, H., and Tamatani, J., Laminar-Turbulent Transition of an Inlet Boundary Layer in a Circular Pipe Induced by Periodic Ejection (Condition for Generating an Isolated Turbulent Patch), *Journal of Fluid Science and Technology*, Vol. 6, No. 6 (2011), pp. 902-915.
(8) Wygnanski, I. J., and Champagne, F. H., On Transition in a Pipe. Part 1. The Origin of Puffs and Slugs and the Flow in a Turbulent Slug, *Journal of Fluid Mechanics*, Vol. 59, Pt. 2 (1973), pp. 281-335.
(9) Bandyopadhyay, P. R., Aspects of the Equilibrium Puff in Transitional Pipe Flow, *Journal of Fluid Mechanics*, Vol. 163 (1986), pp. 439-458.
(10) Darbyshire, A. G., and Mullin, T., Transition to Turbulence in Constant-Mass-Flux Pipe Flow, *Journal of Fluid Mechanics*, Vol. 289 (1995), pp. 83-114.
(11) Priymak, V. G., and Miyazaki, T., Direct Numerical Simulation of Equilibrium Spatially Localized Structures in Pipe Flow, *Physics of Fluids*, Vol. 16, No. 12 (2004), pp. 4221-4234.
(12) Nishi, M., Ünsal, B., Durst, F., and Biswas, G., Laminar-to-Turbulent Transition of Pipe Flows Through Puffs and Slugs, *Journal of Fluid Mechanics*, Vol. 614 (2008), pp. 425-446.
(13) Shimizu, M., and Kida, S., A Driving Mechanism of a Turbulent Puff in Pipe Flow, *Fluid Dynamic Research*, Vol. 41, No. 4, 045501 (2009).
(14) Barkley, D., Simplifying the Complexity of Pipe Flow, *Physical Review E*, Vol. 84, Issue 1, 016309 (2011).
(15) Schubauer, G. B., and Klebanoff, P. S., Contributions on the Mechanics of Boundary-Layer Transition, *NACA Report*, No. 1289 (1956).
(16) Riley, J. J., and Gad-el-Hak, M., The Dynamics of Turbulent Spots, ed. Davis, S. H., and Lumley, J. L., *Frontiers in Fluid Mechanics*, (1985), pp. 123-155, Springer.
(17) Wygnanski, I., Sokolov, M., and Friedman, D., On a Turbulent 'Spot' in a Laminar Boundary Layer, *Journal of Fluid Mechanics*, Vol. 78, Pt. 4 (1976), pp. 785-819.
(18) Cantwell, B., Coles, D., and Dimotakis, P., Structure and Entrainment in the Plane of Symmetry of a Turbulent Spot, *Journal of Fluid Mechanics*, Vol. 87, Pt. 4 (1978), pp. 641-672.
(19) Antonia, R. A., Chambers, A. J., Sokolov, M., and Van Atta, C. W., Simultaneous Temperature and Velocity Measurements in the Plane of Symmetry of a Transitional Turbulent Spot, *Journal of Fluid Mechanics*, Vol. 108 (1981), pp. 317-343.
(20) Wygnanski, I., Zilberman, M., and Haritonidis, J. H., On the Spreading of a Turbulent Spot in the Absence of a Pressure Gradient, *Journal of Fluid Mechanics*, Vol. 123 (1982), pp. 69-90.

(21) Gutmark, E., and Blackwelder, R. F., On the Structure of a Turbulent Spot in a Heated Laminar Boundary Layer, *Experiments in Fluids*, Vol. 5, No. 4 (1987), pp. 217-229.
(22) Ching, C. Y., and LaGraff, J. E., Measurement of Turbulent Spot Convection Rates in a Transitional Boundary Layer, *Experimental Thermal and Fluid Science*, Vol. 11, Issue 1 (1995), pp. 52-60.
(23) Katz, Y., Seifert, A., and Wygnanski, I., On the Evolution of the Turbulent Spot in a Laminar Boundary Layer with a Favourable Pressure Gradient, *Journal of Fluid Mechanics*, Vol. 221 (1990), pp. 1-22.
(24) Clark, J. P., Jones, T. V., and LaGraff, J. E., On the Propagation of Naturally-Occurring Turbulent Spots, *Journal of Fluid Mechanics*, Vol. 28, No. 1 (1994), pp. 1-19.
(25) Narasimha, R., Subramanian, C., and Badri Narayanan, M. A., Turbulent Spot Growth in a Favorable Pressure Gradients, *AIAA Journal*, Vol. 22, No. 6 (1984), pp. 837-839.
(26) Gostelow, J. P., Melwani, N., and Walker, G. J., Effects of Streamwise Pressure Gradient on Turbulent Spot Development, *Transactions of the ASME, Journal of Turbomachinery*, Vol. 118, No. 4 (1996), pp. 737-743.
(27) Seifert, A., and Wygnanski, I. J., On Turbulent Spots in a Laminar Boundary Layer Subjected to a Self-Similar Adverse Pressure Gradient, *Journal of Fluid Mechanics*, Vol. 296 (1995), pp. 185-209.
(28) Zhong, S., Kittichaikan, C., Hodson, H. P., and Ireland, P. T., Visualisation of Turbulent Spots under the Influence of Adverse Pressure Gradients, *Experiments in Fluids*, Vol. 28, No. 5 (2000), pp. 385-393.
(29) Tatsumi, T., Stability of the Laminar Inlet-flow prior to the Formation of Poiseuille Regime, Ⅱ, *Journal of the Physical Society of Japan*, Vol. 7, No. 5 (1952), pp. 495-502.
(30) Huang, L. M. and Chen, T. S., Stability of the Developing Laminar Pipe Flow, *The Physics of Fluids*, Vol. 17, No. 1 (1974), pp. 245-247.
(31) Gupta, S. C. and Garg, V. K., Effect of Velocity Distribution on the Stability of Developing Flow in a Pipe, *The Physics of Fluids*, Vol. 24, No. 4 (1981), pp. 576-578.
(32) Zilberman, M., Wygnanski, I., and Kaplan, R. E. Transitional Boundary Layer Spot in a Fully Turbulent Environment, *The Physics of Fluids*, Vol. 20, No. 10 (1977), pp. S258-S271.
(33) Makita, H., and Nishizawa, A., Interaction between Two Horizontally Displaced Turbulent Spots, *Transactions of the Japan Society of Mechanical Engineers, Series B*, Vol. 64, No. 627 (1998), pp. 3682-3689 (in Japanese).
(34) Terashima, O., Izawa, S., Inasawa, A., and Fukunishi, Y., Streamwise Interface of an Isolated Turbulent Region in a Laminar Flat-Plate Boundary Layer, *Transactions of the Japan Society of Mechanical Engineers, Series B*, Vol. 77, No. 773 (2011), pp. 56-65 (in Japanese).
(35) Glezer, A., Katz, Y., and Wygnanski, I., On the Breakdown of the Wave Packet Trailing a Turbulent Spot in a Laminar Boundary Layer, *Journal of Fluid Mechanics*, Vol. 198 (1989), pp. 1-26.
(36) Rajaratnam, N., *Turbulent Jets* (1976), Elsevier Scientific Publishing, (translated in Japanese, Nomura, Y., *Turbulent Jets* (1981), pp. 178, Morikita Publishing).
(37) Tatsumi, T., Stability of the Laminar Inlet-flow prior to the Formation of Poiseuille Regime, Ⅰ, *Journal of the Physical Society of Japan*, Vol. 7, No. 5 (1952), pp. 489-495.